Conductance of perovskite oxide thin films and interfaces

Mubeen Dildar, I.

4

Carrier density in thin films of doped manganites

In chapter 2 we discussed the physics of La doped manganites in detail. The double exchange mechanism explains the interplay of metallicity and ferromagnetism at low temperatures. At high temperatures, the trapping of electrons occur due to the distortion of oxygen octahedra under the Jahn-Teller effect. The physical properties of these materials largely depend on doping level. The doping of divalent Ca or Sr in the range between 0.2 and 0.5 gives a ferromagnetic metal regime. A ferromagnetic to paramagnetic transition takes place at Curie temperature T_c accompanied by a metal-to-insulator transition at the transition temperature T_p which has practically the same value as T_c. A doping of 0.3 for Ca or Sr gives the highest T_c and T_p. In thin films under strain, T_c and T_p go down, sometimes considerably. In this chapter, we investigate whether the carrier density is affected in very thin films, or when the films are under strain. For this we study the Hall effect.

In this chapter, we study the Hall effect in thin films of $La_{0.7}Ca_{0.3}MnO_3$ and $La_{0.7}Sr_{0.3}MnO_3$ deposited on $SrTiO_3$ (STO), $NdGaO_3$ (NGO) and $LaSrGaO_3$ (LSGO) substrates in a temperature range from below (10 K) to above (400 K) the metal-insulator transition, in magnetic fields up to 9 T, and for thicknesses between 7 nm and 75 nm. The charge carrier density as calculated from the Hall voltage in a single band picture shows bulk-like values for the thick films, but a significant decrease in thin films (below 20 nm), both for strained thin films (on STO) and unstrained thin films on NGO, although less in the case of unstrained films on LSGO. It is well known however that a single band model is not appropriate for the manganites, in which both electron and hole surfaces occur simultaneously. We therefore analyzed the data in a two-band scenario. We still come to the conclusion that the *average* carrier density in the thin films, both strained and unstrained, is lower than in the thicker bulk-like films. We discuss this in terms of charge discontinuities and a possible dead layer at the various interfaces, which appear to play a significant role. We also found conductance anisotropy in transverse direction as a good tool to characterize the homogeneity of thin films of $La_{0.7}Ca_{0.3}MnO_3$ and $La_{0.7}Sr_{0.3}MnO_3$.

4.1 Introduction

Doped manganese perovskite oxides have generated much interest in the last decade, because of the rich physics resulting from the interplay between the electron, lattice, and spin degrees of freedom, and leading to phenomena such as Colossal Magnetoresistance, phase separation, and full spin polarization [1–3]. Considering the La-based 1-1-3 family of manganites, the parent compound $LaMnO_3$ has a structure consisting of 6 corner-sharing MnO_6 octahedra on a simple cubic lattice, encaging the La-ion. It is an antiferromagnetic Mott insulator which can be driven to a metal by partial substitution of divalent Sr^{2+} or Ca^{2+} ions on the La^{3+} sites. The substitution creates holes as charge carriers and above a critical composition of x_c =0.17, a ferromagnetic metallic state forms below the Curie temperature T_c. At a doping level of x=0.3, T_c is around 250 K for $La_{0.7}Ca_{0.3}MnO_3$ (LCMO hereafter) and 370 K for $La_{0.7}Sr_{0.3}MnO_3$ (LSMO). Above T_c the material is a polaronic insulator, and the transition at T_c is therefore both metal-to-insulator (MI) and ferromagnetic-to-paramagnetic. The transition is mainly determined by the competition between the trapping of electrons in Jahn-Teller distortions [4] and the itinerancy of charge carriers through the double exchange mechanism [5, 6]. The sensitivity of the properties of the manganites to lattice distortions is seen in the effects of hydrostatic pressure, which can significantly enhance T_c through rotations of the MnO_6 octahedra [7].

The same sensitivity to lattice distortions makes it possible to apply strain engineering in thin films, by varying the (mis)match between the lattice parameters of film and substrate, as was for instance demonstrated in Refs. [8, 9]. For LCMO in particular, the effects of tensile strain are well documented. Growing LCMO with a pseudocubic lattice parameter of a_c = 0.387 nm on $SrTiO_3$ (STO) with a_c = 0.391 nm can lead to a lowering of T_c of more than 150 K for the thinnest films which still show an MI-transition [10–12]. This is generally attributed to the effect of the decrease of the bandwidth of the itinerant *d*-electrons, due to the change in Mn-O-Mn bond angles and the accompanying decrease of the electron hopping parameter, while also the biaxial nature of the strain plays a role [13]. Such a discussion in terms of the bandwidth of a simple one-band model is not fully correct. Hall-effect measurements on single crystals and thick films consistently show, when analyzed in a one-band model, a higher carrier concentration than the chemical doping indicates (0.3 holes per unit cell for a 2+ doping of 30%). For instance, Asamitsu and Tokura reported a value of 1 hole/Mn site in single crystals of LSMO (30% Sr) [14]; Jacob *et al.* found 0.7 hole/Mn-site in thick films of LCMO (33% Ca) [15]; and Chun *et al.* found values up to 2.4 holes per unit cell in single crystals of $La_{2/3}(Ca,Pb)_{1/3}MnO_3$ [16]. Other reports find similar numbers [17–19]. More than one band is therefore involved in the transport, and this is also indicated by band structure calculations, which find Fermi surfaces with both electron and hole character [20]. Any analysis of Hall data has then to be performed in a scenario of at least two bands, which is not always fully appreciated.

What has not yet been investigated is changes in Hall effect and possibly the carrier density when LSMO or LCMO films become thin and/or strained. This

is relevant, for instance, since microscopic mechanisms advocated to explain the decrease of T_c in strained thin films do not take a possible change of carrier density into account. Also the possibility of valence variations at the interface would make it possible that the carrier density changes when the films become very thin. Here we present results on the ordinary Hall coefficient measured in high magnetic fields, obtained on such films grown strained on $SrTiO_3$ (STO) and unstrained on $NdGaO_3$ (NGO) and $LaSrGaO_3$ (LSGO). We find that, at low temperatures, the one-band hole density $n_{h,1}$ for thick films is found close to 1.5 holes per unit cell, similar to the bulk value and demonstrating again that the Hall coefficient is not a measure for the carrier density when analyzed in a one-band scenario. Below a thickness of typically 20 nm the value of $n_{h,1}$ becomes smaller, and for strained films even goes down to 0.5. In the one-band model this would mean a decrease of the carrier density, but we show that also in terms of a two-band model (in which the mobilities of the various carriers are separate parameters) the conclusion must be that the thin films have a lower carrier density than thick films or bulk material. We argue that this is in line with observations of dead layers and valence variations at the interface.

4.2 Experimental

Epitaxial thin films of LCMO (a_c = 0.3863 nm) and LSMO (a_c = 0.3873 nm) were deposited on substrates of STO(100) (a_c = 0.3905 nm), NGO(100) (a_c = 0.3851 nm; note : this is NGO(110) in orthorhombic notation) and LSGO(100) (a_c = 0.3843 nm) using dc sputtering in pure oxygen at a pressure of 3 mbar. The experimental procedure has been described before [12,21,22] and also in chapter 3. The films ranged in thickness from 7 nm to 75 nm and were characterized by Atomic Force Microscopy (AFM) in tapping mode. A Physical Properties Measurement System (PPMS, Quantum design) was used for the temperature and field control. External current sources and voltmeters were used for the transport measurements of unstructured and structured thin films. The samples were patterned photolithographically into Hall structures. The bridges were 200 μm in width and 3.6 mm in length while the distance between two voltage contacts was 1.2 mm. Argon Ion Beam Etching (etch rate 0.3 nm/sec) was used for structuring the LCMO films, and wet etching (H_2O: HF: HCl: HNO_3 = 25: 1: 1: 1) with an etch rate of 2 nm per second for the LSMO thin films. After Ar-Etching, the LCMO samples were treated with oxygen plasma in order to restore the insulating properties of the STO substrate [22]. For the measurements of the Hall coefficient, the temperature was stabilized to better than 20 mK. The data were taken at constant temperature, with a current between 1 mA and 100 μA. A full current-voltage measurement was made regularly to check linearity and the absence of an offset. The magnetic field (oriented perpendicular to the sample plane) was scanned from -9 T to +9 T, which takes about 3 hours.

4.3 Results

In this section, we present the morphology of the films, XRD and RSM maps, and resistivity measurements. High resolution XRD measurements were performed in Twente University in collaboration with Dr. S. Harkema.

4.3.1 Characterization by AFM

Figure 4.1a,b shows morphology and height variation of a 16 nm thick film of LCMO on STO called L583. The film is flat, and shows step-height variations of the order of a unit cell (0.4 nm), together with the beginning of spiral growth. Figure 4.1c,d shows the surface morphology and the height variation along a cross-section of a 25 nm thick film of LSMO on STO, called LS8. Again, height variations are not more than 0.4 nm.

4.3.2 Characterization by RSM

The film thickness was measured by x-ray reflectivity, using Cu-Kα radiation, where the thickness of the film is defined by the period of oscillation. Films grown on STO are strained (mismatch: -1.07% in case of LCMO and -0.82% in case of LSMO), although the strain gradually relaxes with increasing thickness [21].

Figure 4.2 shows a reciprocal space map for the 25 nm thick film LS8 of LSMO on STO around the [123] reflection. The film is strained and epitaxial. Along the out-of-plane direction a clear film peak is visible separate from the substrate peak, while the in-plane direction shows the same peak values for substrate and film peak. The out-of-plane lattice parameter was determined with this reflection as well as the [002] and [003] reflections, and found to be 0.386 nm, well below the bulk value of 0.389 nm. Films of LCMO with a thickness below 20 nm, grown around the same time as the samples reported on here, showed an out-of-plane lattice parameter around 0.381 nm, much reduced from the pseudocubic bulk value, and confirming that such films are fully strained. Films on NGO (mismatch: less than 0.3% in case of LCMO and LSMO) are slightly tensile strained and on LSGO (mismatch: 0.52% in case of LCMO and 0.78% in case of LSMO) are slightly compressive.

4.3.3 Resistivity measurement

Figure 4.3a shows the temperature dependence of the longitudinal resistance $R(T)$ of structured films of LCMO for different thicknesses on different substrates (9 nm, 16 nm, 75 nm on STO, 16 nm on LSGO). Data are given both for zero field, and in a field of 9 T. The behavior is as reported before: the thinnest film on STO shows a peak temperature of the resistance T_p around 130 K, which then increases to 200 K for the 75 nm film. The films on better matching substrates show higher value of T_p, even though they are very thin. Figure 4.3b shows similar data for LSMO (LS15 with thickness 7 nm, LS8 with thickness 25 nm, a film of 75 nm) on STO. The effects of strain on LSMO are less strong, as can be seen from the fact

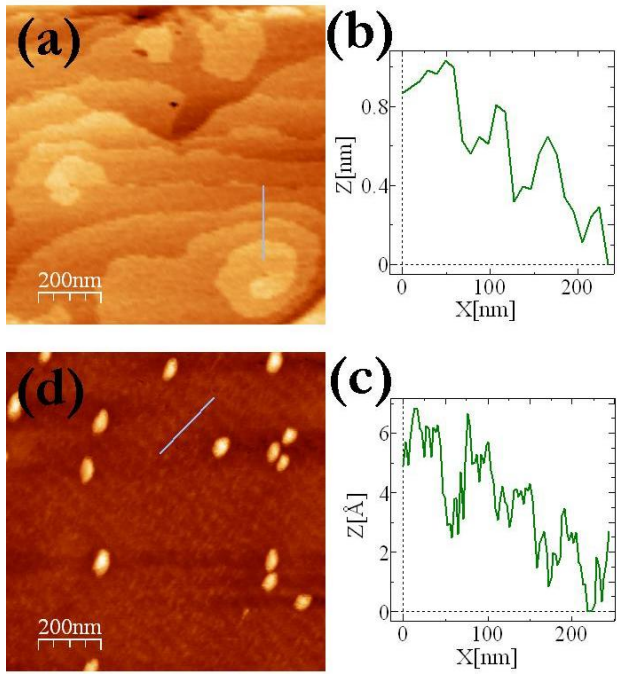

Figure 4.1: Surface morphology of (a) a 16 nm thick film of LCMO on STO (called L583); (c) a 25 nm thick film of LSMO on STO (called LS8). The panels (b) and (d) show the height variation along the lines given in (a) and (c), respectively.

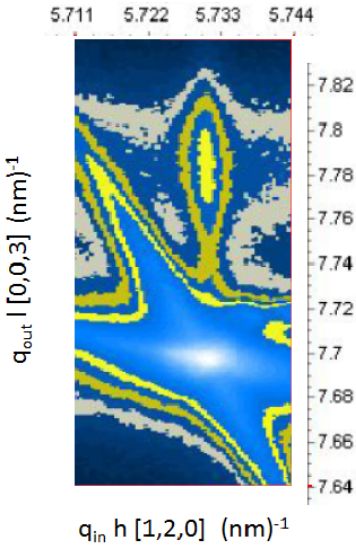

Figure 4.2: Reciprocal space map of a 25 nm thick film of LSMO on STO (called LS8), taken around the [123] reflection. The film peak can be seen at $q_{out} \approx 7.78$ nm^{-1}.

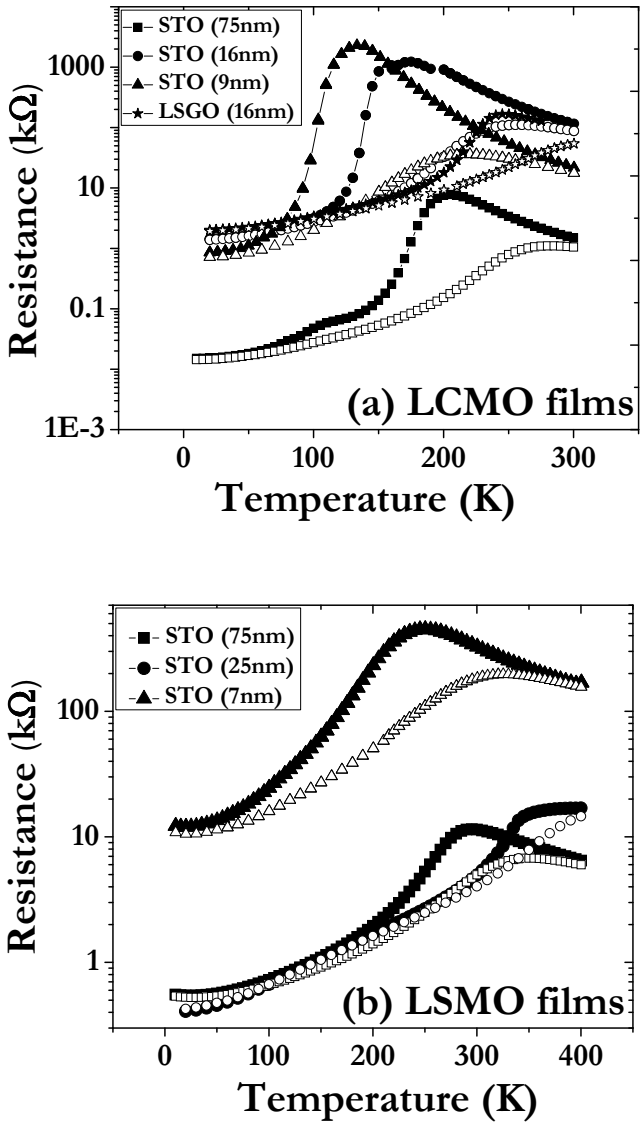

Figure 4.3: Resistance R versus temperature T in zero field and in a 9 T field of structured films of $La_{0.7}Ca_{0.3}MnO_3$ (LCMO) and $La_{0.7}Sr_{0.3}MnO_3$ (LSMO) of different thickness on different substrates. (a) LCMO: 9 nm, 16 nm, 75 nm on STO, 16 nm on LSGO. (b) LSMO: 7 nm (LS15) , 25 nm (LS8), 75 nm on STO. The filled symbols show 0-field data, the open symbols show data taken in 9 T.

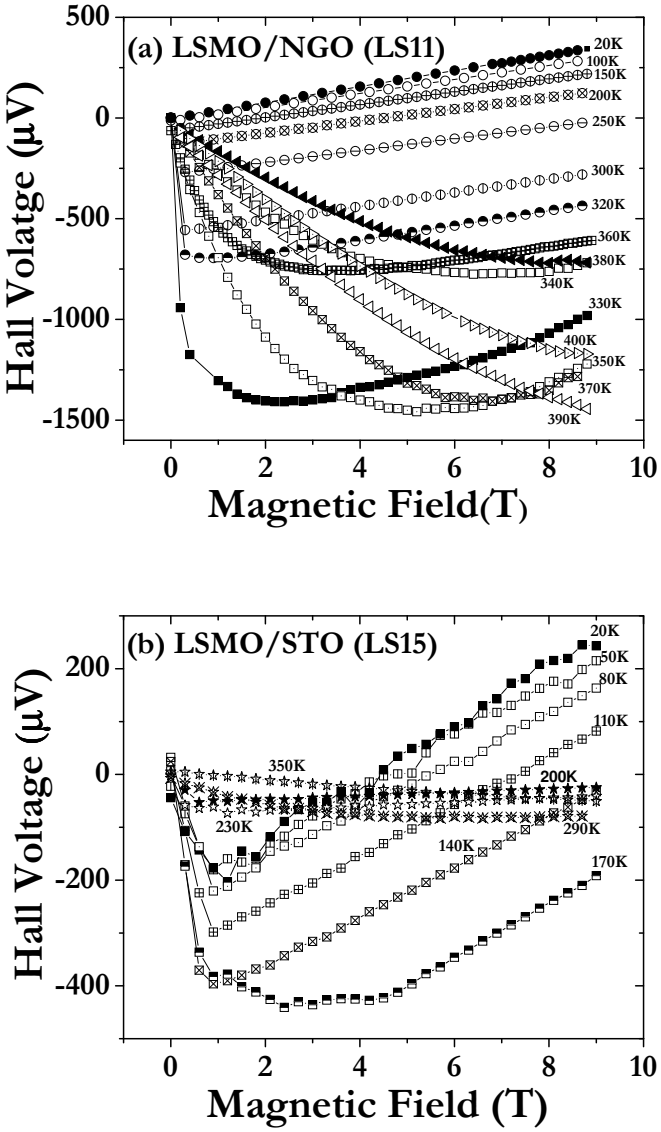

Figure 4.4: Hall voltage as function of magnetic field at constant temperature (as indicated) for the film of (a) 13 nm LSMO on NGO, called LS11. (b) 7 nm LSMO on STO, called LS15. The data is divided in three regimes; first regimes (indicated by circles) where Hall voltage is completely linear, 2nd regime (indicated by squares) both anomalous and linear part of Hall voltage, 3rd regime (triangles) behavior is totally anomalous.. For thin film on STO, the first region is missing and the anomalous behavior already starts at low temperature.

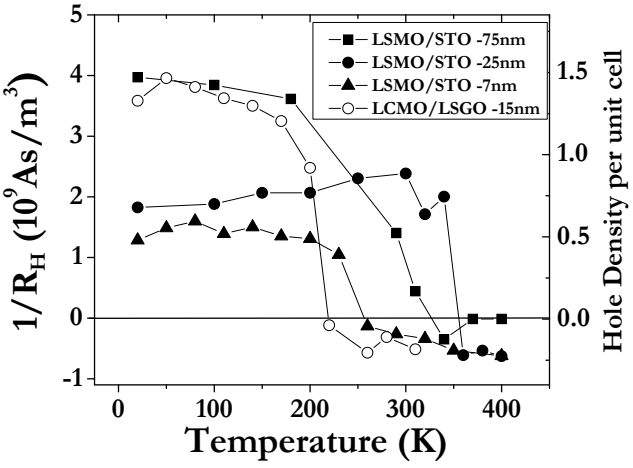

Figure 4.5: Inverse Hall resistance R_H (left hand scale) and hole density per unit cell (right hand scale) as function of temperature, for LSMO films with thicknesses 7 nm (LS15), 25 nm (LS8), 75 nm on STO, and an LCMO film of 15 nm on LSGO.

that T_p for the 25 nm film is already close to the bulk value. The high field data show the usual Colossal Magnetoresistance effect.

Next, the Hall voltage U_H was measured on these films as function of the magnetic field H_a applied perpendicular to the plane of the sample, and at different constant temperatures. In all cases the offset voltage was low, except for the case of 9 nm LCMO on STO. That sample will not be considered further. Figure 4.4 shows U_H for LS15 (the 7 nm film of LSMO on STO), as determined by taking the average of the measured voltage at $+H_a$ and $-H_a$. For this film T_p is around 230 K. Below T_p, U_H as function of increasing field first drops down, and then increases linearly. Around and above T_p, the crossover to linear behavior becomes less pronounced, and vanishes above 230 K. The behavior below T_p is usually understood from the relation

$$\rho_H = \frac{E_H}{J} = \frac{U_H d_F}{I} = \mu_0(R_H H_a + R_A M) \tag{4.1}$$

Here, E_H is the electric field, J the current density, I is the current, d_F is the film thickness, R_H the ordinary Hall coefficient and R_A the anomalous Hall coefficient. That can be due to the magnetization [23], but in manganites R_A appears to have a different origin, since its contribution grows with increasing temperature right up to the transition temperature. This behavior is well documented [15, 16, 18] and was ascribed to the carriers moving in a non-trivial background of core spins [24]. The positive slope seen in the data of Figure 4.4 signifies the hole character of the carriers. The value for R_H is determined from the linear part of the data for $U_H(H_a)$. For instance, at 20 K the slope is about 53 μV/T which, with a thickness

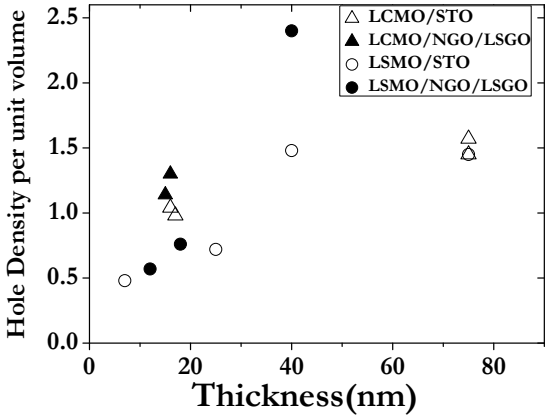

Figure 4.6: One-band hole density $n_{h,1}$ versus film thickness. Filled symbols show films on NGO/LSGO (triangles: LCMO; circles: LSMO), empty symbols show films on STO

of 7 nm and a measurement current of 500 μA yields $R_H = 7.5 \times 10^{-10}$ m^3/As. In a single band picture, the carrier density directly follows from $n_c = V_{uc}/(eR_H)$, with V_{uc} the unit cell volume and e the electron charge. Around T_c there is no large linear regime, and there we used the high-field part of the data above roughly 6 T. We are mainly interested in the low-temperature carrier density, but in this way the transition is clearly visible. In Figure 4.5, we show a representative set of data taken from different film-substrate combinations of $1/R_H$ and the hole density $n_{h,1}$ evaluated in a one band picture. In all cases there is a relatively steep rise around T_c of the film, followed by saturated behavior to low temperatures. At low temperatures, the 75 nm LSMO film on STO shows a value of $n_{h,1} \approx 1.5$, in line with previous reports on thick films. The 16 nm LCMO film on LSGO has $n_{h,1} \approx 1.3$, slightly lower than the bulk. The thin strained films deposited on STO show values around 0.7. In Figure 4.6 the values of $n_{h,1}$ for all samples are collected, taken at 20 K. The values and other characteristics of all samples are also collected in Table 4.1.

4.3.4 Hall Offset as a homogeneity parameter

A question which can be raised is whether these very thin and small films pose homogeneity problems which may yield inhomogeneous current distributions. It was noticed that for thin films of LCMO, less than 12 nm, it is not possible to perform reliable measurements because of the very large resistance at low temperature. Here, we find a relation between Hall offset and homogeneity of thin films of LSMO and LCMO.

Hall measurements always show a small offset. To avoid this offset, a magnetic

Film	substrate	thickness nm	T_p K	$1/R_H$ 10^9 C/m^3	$n_{h,1}$	$n_{h,2}$	μ_e/μ_h
LSMO	STO	75	325	4.0	1.45	0.55	0.8
LSMO	STO	40	370	4.1	1.48	0.55	0.8
LSMO	STO	25	370	2.0	0.72	0.32	0.3
LSMO	STO	7	250	1.3	0.48	0.2	0.3
LSMO	NGO	12	370	1.6	0.57	0.25	0.3
LSMO	STO	18	365	2.1	0.76	0.35	0.3
LSMO	STO	40	375	6.8	2.4	0.55	1.5
LCMO	STO	75	190	4.0	1.45	0.55	0.8
LCMO	STO	75	210	4.3	1.57	0.55	0.9
LCMO	STO	17	175	2.7	0.98	0.45	0.3
LCMO	STO	16	175	2.85	1.04	0.46	0.3
LCMO	NGO	15	210	2.9	1.14	0.53	0.3
LCMO	LSGO	15	245	3.7	1.3	0.55	0.7

Table 4.1: The Table shows type of film; type of substrate; film thickness; peak temperature T_p; the value of $1/R_H$ taken at 20 K, and the corresponding value of the one-band hole density $n_{h,1}$. It also show the two-band hole density $n_{h,2}$ and the mobility ratio μ_e/μ_h determined in the following way: if $n_{h,2}$ can be fixed to 0.55, the mobility ratio is a free parameter; if no mobility ratio can be found to match 0.55, the ratio is fixed at 0.3.

field is applied in both directions and then averaging $+\triangle V_H$ and $-\triangle V_H$ gives the actual Hall voltage U_H. In the absence of magnetic field, the Hall offset (measured in Ohm) is found to be a good parameter to check the homogeneity of thin films of LSMO and LCMO.

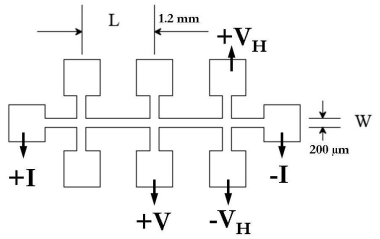

Figure 4.7: A standard Hall bar used to measure resistance in longitudinal configuration (shown as +V and $-V_H$) and in Hall configuration (shown as $+V_H$ and $-V_H$).

Figure 4.8 shows the resistance measured in longitudinal configuration and Hall configuration (both are sketched in Figure 4.7) for a 12 nm thin film of LSMO on NGO. The longitudinal measurement shows T_{MI} at 380 K while the Hall offset follows the same trend but the resistance is about 2% of the longitudinal resis-

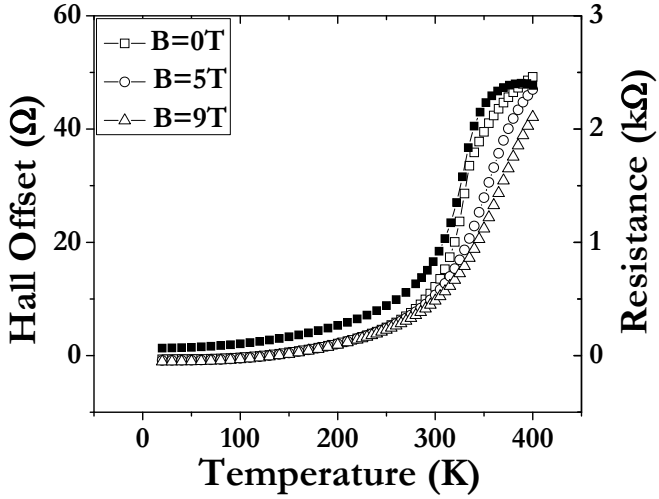

Figure 4.8: (Left axis, open symbols) Hall offset versus temperature in zero field, 5 T and 9 T for a 13 nm thin films of LSMO on NGO (LS11), (right axis, filled symbols) longitudinal resistance of the same sample.

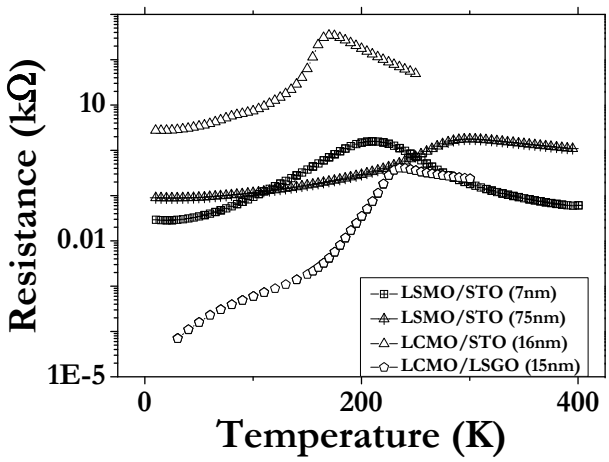

Figure 4.9: Temperature dependence of Hall offset for LSMO and LCMO films.

tance. Applying a magnetic field shows a small reduction in the Hall offset above 250 K. This is the first region in Figure 4.8a where the Hall voltage was found to be perfectly linear with the applied field. This behavior (reduced resistance and $\pm T_{MI}$) is found in all films of LSMO and LCMO except less than 15 nm films of LCMO.

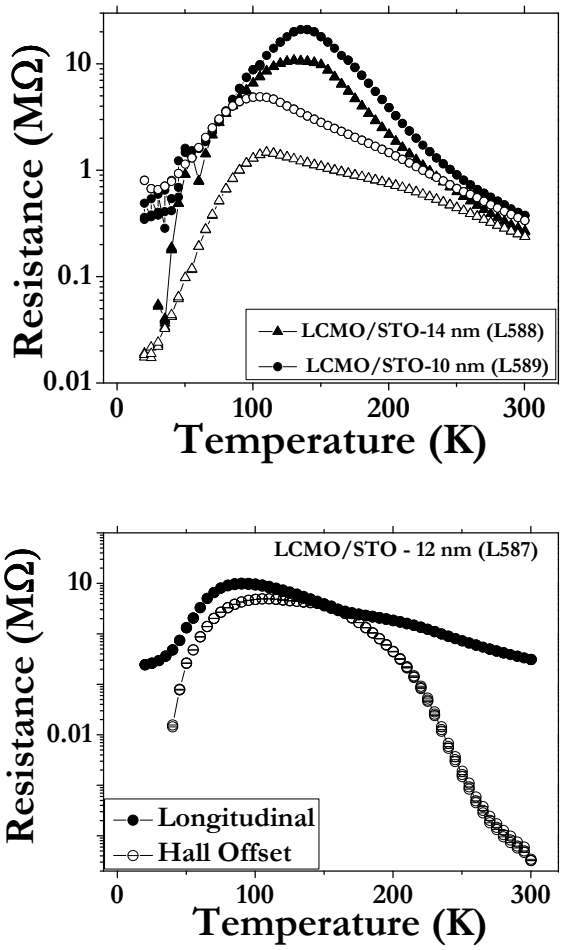

Figure 4.10: (a) Longitudinal resistance versus temperature for two films of LCMO on STO, a 14 nm (L588) and a 10 nm (L589) measured at 0 T (shown with filled symbols) and at 9 T (shown with open symbols), (b) Resistance versus temperature behavior for a 12 nm film measured in longitudinal and in Hall offset mode.

We showed in Figure 4.3 the resistance dependence on temperature for thin

films of LSMO and LCMO at 0 T and at 9 T. The Hall offset of these films is presented in Figure 4.9. For all homogenous LSMO and LCMO films, the Hall offset gives the T_{MI} with ±40 K change as compared to T_{MI} measured in the longitudinal measurements. The main difference is that the resistance in the Hall offset is 50 times lower than the longitudinal resistance. The resistance in Hall offset increases for thin films but remains measurable. Ultrathin films of LCMO, less than 15 nm, show homogeneity problem because the resistance becomes very high at low temperature and the effect of the magnetic field is not as strong as in thicker films, as shown in Figure 4.10a. In these thin films, measuring the Hall offset gives a resistance with values very similar to the longitudinal resistance as shown in Figure 4.10b. We also find that for these films, it was not possible to measure linear U_H while for LSMO, even 7 nm thin film gives linear data as shown in Figure 4.4b. In LCMO thin films, a large resistance measured in Hall offset configuration cannot be only because of misalignment of contacts. Inhomogeneities persist in narrow bandwidth LCMO thin films more than the wider bandwidth LSMO and the charge carriers can be not dragged away due to inhomogeneous current distribution to measure U_H for thinner films.

4.4 Discussion

As we noted above, a one band picture is not appropriate to discuss Hall data. For a more complete discussion, we use the same starting point as done before, namely the band structure calculations of Pickett and Singh. They found a hole pocket of cubic shape, containing 0.55 holes and centered around the R-point of the Brillouin zone (the corner point of a simple cube); and an electron pocket of spherical shape, containing 0.05 electrons and centered around the Γ point [20,25]. This was confirmed by other calculations as well as by several experiments. In particular Livesay *et al.* reported similar calculations and experimentally verified the presence and shape of both Fermi Surfaces (FS) by positron annihilation [26] on a single crystal of $La_{0.7}Sr_{0.3}MnO_3$. Photoemission studies on thin films (40 nm) of $La_{1-x}Sr_xMnO_3$ grown on NGO confirmed the existence of the Γ-centered electron pocket for $x = 0.3$ [27]. This film was sightly strained, and it is important to note that in such films this part of the FS still exists. In photoemission no clear evidence is found for the hole-type FS, as discussed in Ref. [28].

In the two-band picture, the relation between the measured Hall resistance R_H and the two carrier densities is as follows:

$$R_H = \frac{r_h n_h \mu_h^2 - r_e n_e \mu_e^2}{e(n_h \mu_h + n_e \mu_e)^2} \tag{4.2}$$

Here, $n_{h,e}$ are the hole, electron densities, $\mu_{h,e}$ are the hole, electron mobilities, and $r_{h,e}$ are factors taking the shape of the FS into account, with $r = 1$ for a spherical surface and $r = 1/2$ for a cubic surface [29]. The shape factors were used by Chun *et al.* in their analysis [16], but not by Jacob *et al.* [15], nor by Bibes *et al.* [30]. For our analysis, the shape factors turn out to be important.

In order to work with Eq. 4.2, several assumptions have to be made. Taking the Pickett-Singh carrier densities, we can resolve for the mobility ratio μ_e/μ_h using the measured R_H. For the three 75 nm LCMO and LSMO films on STO, we find mobilities ratio's of 0.8 and 0.9, which is of the same order of magnitude as found before [16]. The actual numbers are given in Table 4.1.

When we try the same for the data with lower values of $1/R_H$ (and therefore n_h) however, we cannot find reasonable values for μ_e/μ_h which would reproduce the Picket-Singh densities of 0.55 (n_h) and 0.05 (n_e). This is shown pictorially in Figure 4.11 where we plot the values of $n_{h,2}$ versus $V_{uc}/(eR_H) = n_{h,1}$ for different values of μ_e/μ_h.

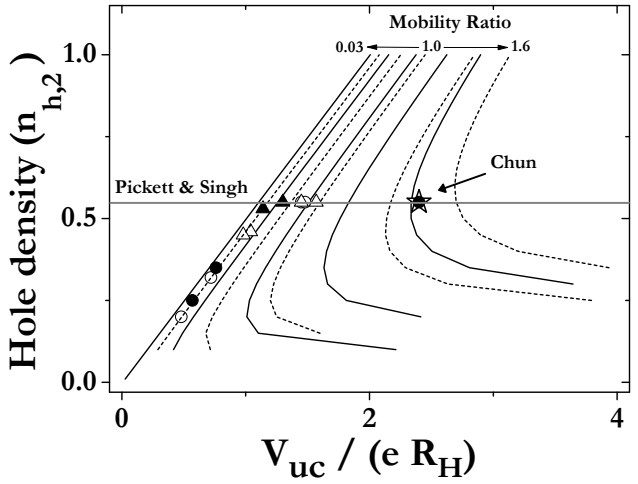

Figure 4.11: The two-band hole density $n_{h,2}$ plotted as function of V_{uc}/eR_H, with the contours showing different values of the mobility ratio μ_e/μ_h. Contours are given at mobility ratios 0.03, 0.3, 0.5, 0.7, 0.9, 1.0, 1.2, 1.4, 1.5, 1.6. For $V_{uc}/(eR_H)$ $= n_{h,1} > 1.2$, its value is fixed at the Pickett-Singh value of 0.55. Below $n_{h,1} = 1.2$, data are plotted on the $\mu_e/\mu_h = 0.3$ contour. Filled symbols show films on NGO / LSGO (triangles: LCMO; circles: LSMO), empty symbols show films on STO. The single crystal data of Chun et al [16] is plotted with an asterisk.

The Figure firstly shows the solution of Chun *et al.* for their single crystal, namely a mobility ratio of about 1.5 at a Hall resistance corresponding to $n_{h,1} =$ 2.4. It also shows the asymptote which is found when μ_e/μ_h goes to zero, which is the reason that for values below roughly $V_{uc}/(eR_H) = n_{h,1} = 1.2$, no solution can be found which reproduces the Pickett-Singh carrier densities. For the 75 nm samples, the mobility ratio is seen to be about 1. For samples with $n_{h,1}$ below 1.2 we plot them at a mobility ratio of 0.3, which means we allow for a factor 3 change in the ratio. As can be seen in the Figure, this leads to a decrease of

$n_{h,2}$ from 0.55 to about 0.25. The conclusion from the analysis therefore is that in the 2-band model, and using $r = 1/2$, the data in particular for the thinnest films cannot be described by changing only the mobility ratio, but that the carrier density also has to be lower. This is somewhat different when $r = 1$ is used for the hole pocket. Solutions are then possible down to $n_{h,1} \approx 0.6$. However, the single crystal experiments of Chun *et al* cannot be described in this way, and the spread of mobility ratio's which describe our samples becomes large : from 0.3 at $n_{h,1} =$ 0.6 to 2.5 at $n_{h,1} = 1.5$, roughly an order of magnitude, while the 7 nm LSMO on STO still cannot be described.

Generally, the LSMO films show a significantly decreased carrier density even when the mobility ratio is lowered to 0.3, while the LCMO films show a smaller decrease, of the order of 10%. However, lowering the value of μ_e/μ_h from 1.5 to 0.3 is not completely physical, because of the following. From the band structure calculations it was found that the holes are very light ($m_h \approx 0.6m^*, m^*$ the bare electron mass), while the electrons are very heavy ($m_e \approx 14m^*$). A lower μ_e/μ_h would mean a still *larger* value of m_e and/or a still *smaller* value of m_h, which seems unlikely. On the other hand, a higher μ_e/μ_h means a lower carrier density. The analysis therefore strongly indicates that for both LSMO and LCMO films the carrier density of films of roughly 20 nm or less is significantly smaller than in the bulk. The one exception is the 15 nm LCMO film on LSGO, which can be described with parameters still close to the bulk values.

For all substrate/film combinations, therefore, the number of measured carriers becomes smaller for thin films, also in the field of 9 T used in the measurements. Looking separately at LSMO and LCMO, we see from Table 4.1 that for LSMO, there is a monotonic decrease of $\mathrm{n}_{h,2}$ with thickness, and that the film on NGO does not behave differently from the films on STO. Here we come back to the issue of the dead layers, already signaled in section 2.3.2. Such a dead layer of about 4 nm is well documented for LSMO/STO [31] and LSMO/NGO [32]. If we assume that this layer does not contribute carriers (even in 9 T), but that above the critical thickness d_{cr} the carrier contribution is bulk like, then the thickness-averaged carrier density is given by $\bar{n}_{2,h} = \mathrm{n}_{2,h}^{bulk}$ (1 - d_{cr}/d). At the smallest thickness of 7 nm, this leads to an average value of 0.4 times the bulk value, in very good agreement with the number from the analysis.

Also for LCMO, dead layers of the order of 5 nm have generally been reported [11, 21]. In this case the analyzed reduction at 15 nm is less, of the order of 10 % - 20 %, and also less than the 30 % which might be expected on the basis of the dead layer. Assuming that the mobility ratio has changed less than to 0.3 would remedy this. On the whole, the data indicate that both for wider and smaller bandwidths, and irrespective of strain, the interface effects are significant, and stretch over a number of nanometers. The cause of this effect may well lie in a charge transfer due to a charge discontinuity, very similar to what is intensively researched on the LAO/STO interface [36]. Just as the polar $LaAlO_3$ consists of charged blocks of $(LaO)^{1+}$ and $(AlO_2)^{1-}$, the LSMO layer consists of blocks $[(La_{0.7}Ca_{0.3}O_3]^{0.7+}$ and $(MnO_2)^{0.7-}$ which cause a charge discontinuity at the interface with STO. In the case of LSMO/STO dead layer, an explanation was given in terms of an

orbital reconstruction [33], accompanied by a slight increase in the amount of Mn^{3+} ions [34]. We have similar evidence of Mn^{3+} enrichment from Electron Energy Loss Spectroscopy (EELS) at the interface of LCMO/STO [35]. Particularly interesting in this respect is the case of LCMO on LSGO, where we do not find carrier loss, since this would also fit the charge discontinuity picture. For LAO and NGO, the charge of the blocks is (+1,-1). For LSGO it is half that value, because of the mixed La,Sr valence, and therefore closest in charge matching to the LSMO layer. The LSGO substrate is therefore expected to give the smallest effect.

In conclusion, the data fit a model in which an active manganite layer occurs above a critical thickness. This active layer contains a bulk-like amount of carriers, although T_p can be significantly lower, which is the result of strain.

4.5 Anomalous Hall effect

In ferromagnetic materials, an additional voltage is produced due to the embedded magnetic moments which causes asymmetric scattering of current carrying electrons, called anomalous Hall voltage. The anomalous Hall coefficient, denoted as R_A in Eq. 4.1 has a straightforward relation with the Hall resistivity but is theoretically difficult to explain, and has remained poorly understood. The anomalous Hall effect (AHE) in manganites for thick films [15, 30] and single crystals [14, 16] was studied but not in thin films of manganites. In chapter 2, we gave some the background and theories related to anomalous Hall effect. In this section, we discuss the contribution of anomalous Hall effect (AHE) in thin films of LSMO and LCMO.

We saw in Figure 4.4 that in the low temperature and high field regime, the anomalous contribution is minimum because of saturation of magnetic domains. The Hall voltage remains linear and we find out the ordinary Hall co-efficient R_H almost constant. With increase in temperature, R_H increases and R_A also increases. In the low field regime, the anomalous Hall contribution is dominant and it arises from two different elementary processes, skew scattering and side jump. Skew scattering describes the average deflection of the trajectory of a charge carrier in a scattering event and a side jump mechanisms is ascribed to the displacement of the trajectory from its original path through the scattering center. These two processes are linked to the longitudinal resistivity and anomalous Hall coefficient through a power law $R_A \mu_o M = \gamma \rho_{xx}^n$. For the skew scattering process, n=1 while n = 2 for the side jump mechanism. To find the value of n in thin films, we rearrange Eq. 4.1 as

$$\rho_H^* = \mu_0 R_A M \tag{4.3}$$

where $\rho_H^* = \rho_H - \mu_0 R_H H_a$.

For all grown films shown in Table 4.2, the Curie temperature and saturation magnetization were measured as shown in Figure 4.12. The anomalous Hall contribution is determined by extrapolating the linear high field data at 9 T, back to zero field. A double logarithmic plot of ρ_H^* (9 T) versus $R_A = \rho_H^*/(\rho_H M_{sat})$

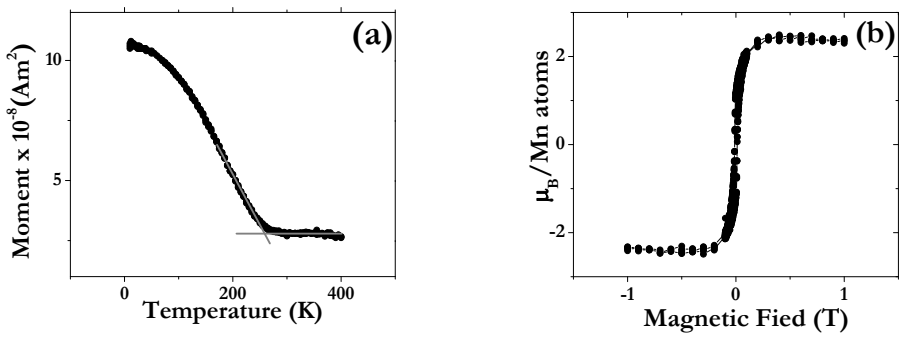

Figure 4.12: (a) Temperature dependence of magnetization for a 7 nm thin film of LSMO on STO (LS15) (b) Field versus magnetization for the same film shown in (a) at 10 K.

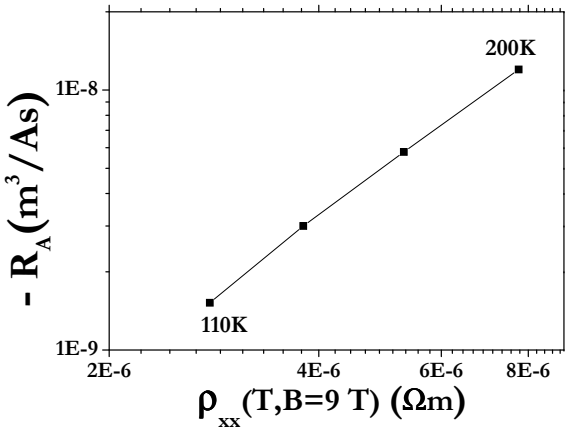

Figure 4.13: Anomalous Hall coefficient versus longitudinal resistivity ρ_{xx} at B= 9 T for a 15 nm thin film of LCMO on LSGO.

is plotted in Figure 4.13 for a 15 nm thin film of LCMO on LSGO (L600). This gives a perfect power law in the ferromagnetic regime, with an exponent n = 2. To take in account the magnetoresistive effects, data points at temperatures close to T_c and T_p are included and smaller than 50 K are excluded to find out power factor [15]. We have determine the power n for thin films of LSMO and LCMO on STO and LSGO substrates as shown in Table 4.2. We observe that thick films of LSMO and LCMO (75 nm) on STO as well as LCMO on LSGO give $1.5 \leq n \geq 2.1$. The same value for n is found in literature and it is claimed that the side

jump mechanisms is dominant in manganites [15]. For thin films which are strained and show a reduction in *average* carrier density, the power factor n is close to 1. The skew scattering seems to play a role in thin strained films. It is required to develop theoretical models to find out the scattering mechanisms in very thin films of manganites.

Film	substrate	thickness nm	T_p K	T_c K	μ_B/Mn	$n_{h,1}$	n
LSMO	STO	75	325	312	2.4	1.45	2.1
LSMO	STO	25	370	340	2.5	0.72	1
LSMO	STO	7	250	243	2.1	0.48	0.9
LCMO	STO	75	190	177	2.8	1.45	1.5
LCMO	STO	75	210	200	2.8	1.47	1.6
LCMO	STO	16	175	170	2.4	1.04	1.0
LCMO	LSGO	15	245	242	2.1	1.3	2

Table 4.2: The Table shows type of film; type of substrate; film thickness; peak temperature T_p; Curie Temperature (K) at 1 mT for all films except for 25 nm LSMO on STO which was measured at 10 mT; Bohr magneton μ_B/Mn, hole density $n_{h,1}$ in one band model and power factor n, related to Hall and longitudinal resistivity.

4.6 Conclusion

In conclusion, we have shown that, even though the inverse Hall constant cannot be directly connected to a carrier density since a one band picture does not apply, also an analysis in a two-band scenario shows that the *average* carrier density decreases both in LSMO and LCMO films when they become thinner. Strain does not appear to be the main driver. Rather, the data taken with different substrates indicate interface effects, in line with current models for charge discontinuities. The range of these effects appears to be a few nanometer. The utilization of Hall offset for homogeneous thin films is described. The AHE is found to have different scattering processes for thicker/relaxed and thin/strained films.

Bibliography

[1] E. Dagotto, T. Hotta, and A. Moreo, Phys. Rep. **344**, 1 (2001)

[2] M.B. Salamon and M. Jaime, Rev. Mod. Phys. **73**, 583 (2001).

[3] Y. Tokura, Rep. Prog. Phys. **69**, 797 (2006).

[4] A.J. Millis, Nature **392**, 147 (1998).

[5] C. Zener, Phys. Rev. **82**, 403 (1951).

[6] P.W. Anderson and H. Hasegawa, Phys. Rev. **100**, 67 (1955).

[7] H.Y. Hwang, T.T.M. Palstra, S.-W. Cheong and B. Batlogg, Phys. Rev. B **52**, 15046 (1995).

[8] Y. Konishi, Z. Fang. M. Izumi, T. Mamako. M. Kasai, H. Kuwahara, M. kawasaki, K. Terakura and Y. Tokura, Jn. Phys. Soc. Japan **68**, 3790 (1999).

[9] Z. Fang, I.V. Solovyev, and K. Terakura, Phys. Rev. Lett. **84**, 3169 (2000).

[10] J. Aarts, S. Freisem, R. Hendrikx and H.W. Zandbergen, Appl. Phys. Lett. **72**, 2975 (1998).

[11] M. Bibes, Ll. Balcells, S. Valencia, J. Fontcuberta, M. Wojcik, E. Jedryka, and S. Nadolski, Phys. Rev. Lett. **87**, 067210 (2001).

[12] Z.Q. Yang, R. Hendrikx, J. Aarts, Y.L. Qin and H.W. Zandbergen, Phys. Rev. B **70**, 174111 (2004).

[13] A.J. Millis, T. Darling and A. Migliori, J. Appl. Phys. **83**, 1588 (1998).

[14] A. Asamitsu and Y. Tokura, Phys. Rev. B **58**, 47 (1998).

[15] G. Jakob, F. Martin, W. Westerburg and H. Adrian, Phys. Rev. B **57**, 10252 (1998).

[16] S.H. Chun, M.B. Salamon and P.D. Han, Jn. Appl. Phys. **85**, 5573 (1999).

[17] G.J. Snyder, R. Hiskes, S. DiCarolis, M.R. Beasley and T.H. Geballe, Phys. Rev. B **53**, 14434 (1996).

[18] P. Matl, N.P. Ong, Y.F. Yan, Y.Q. Li, D. Studebaker, T. Baum and G. Doubinina, Phys. Rev. B **57**, 10248 (1998).

[19] N.G. Bebenin, R.I. Zainullina, N.S. Bannikova, V.V. Ustinov, Y.M. Mukovskii, Phys. Rev. B **68**, 064415 (2008).

[20] W.E. Pickett and D.J. Singh, Phys. Rev. B **55**, R8642 (1997).

[21] Z.Q. Yang, R. Hendrikx, J. Aarts, Y. Qin, and H.W. Zandbergen, Phys. Rev. B **67**, 024408 (2003).

[22] C. Beekman, I. Komissarov, M. Hesselberth and J. Aarts, Appl. Phys. Lett. **91**, 062101 (2007).

[23] R. O`Handley, Modern Magnetic Materials, Wiley and Sons, New York, 2000.

[24] J. Ye, Y.B. Kim, A.J. Millis, B.I. Shraiman, P. Majumdar, and Z. Tesanovic Phys. Rev. Lett. **83**, 3737 (1999).

[25] W.E. Pickett and D.J. Singh, Jn. Magnetism and Magn. Materials **172**, 237 (1997).

[26] E.A Livesay, R. N West, S. B Dugdale, G. Santi and T. Jarlborg, J. Phys. Cond. Mat. **11**, l279 (199).

[27] A. Chikamatsu, H. Wadati, H. Kumigashira, M. Oshima, A. Fujimori, M. Lippmaa, K. Ono, M. Kawasaki and H. Koinuma, Phys. Rev. B **76**, 201103 (2007).

[28] M. Shi, M.C. Falub, P.R. Willmott, J. Krempasky, R. Herger, L. Patthey, K. Hricovini, C.V. Falub and M. Schneider, J. Phys. Cond. Mat. **20**, 222001 (2008).

[29] R.S. Allgaier, Phys. Rev. **165**, 775 (1968).

[30] M. Bibes, V. Laukhin, S. Valencia, B. Martínez, J. Fontcuberta, O. Yu. Gorbenko, A. R. Kaul, and J L Martínez, J. Phys. Cond. Mat. **17**, 2733 (2005).

[31] M. Huijben, L.W. Martin, Y.-H. Chu, M.B. Holcomb, P. Yu, G. Rijnders, D.H.A. Blank, and R. Ramesh, Phys. Rev. B **78**, 094413 (2008).

[32] J.Z. Sun, D.W. Abraham, R.A. Rao, and C. Eom, Appl. Phys. Lett. **74**, 3017 (1999).

[33] A. Tebano, C. Aruta, S. Sanna, P.G. Medaglia, G. Balestrino, A.A. Sidorenko, R. De Renzi, G. Ghiringhelli, L. Braicovich, V. Bisogni and N.B. Brookes, Phys. Rev. Lett. **100**, 137401 (2008).

[34] J.-S. Lee, D.A. Arena, P. Yu, C.S. Nelson, R. Fan, C.J. Kinane, S. Langridge, M.D. Rossell, R. Ramesh, and C.-C. Kao, Phys. Rev. lett. **105**, 257204 (2010).

[35] C. Beekman, M. Porcu, and H.W. Zandbergen, and J. Aarts, arXiv:1102.4004v1 [cond-mat.mes-hall].

[36] O. Ohtomo and H.Y. Hwang, Nature **427**, 423 (2004).